EasyChair Preprint

№ 417

Fracture mechanic and charpy impact properties of a crack in weld metal, HAZ and base metal of welded armor steel

Aleksandar Čabrilo and Katarina Gerić

August 9, 2018

Fracture mechanic and charpy impact properties of a crack in weld metal, HAZ and base metal of welded armor steel

Aleksandar Cabrilo[a]*, Katarina Geric[a]

Faculty of Technical Sciences, Trg Dositeja Obradovica 6, Novi Sad 21000, Serbia

Abstract

Welding of armored steel is complicated by the high percentage of carbon in the base metal, the presence of defects in the form of cracks and pores that occur in the weld metal and heat affected zone (HAZ) during the welding process. For heavy structural engineering such as military armored vehicles that are frequently under the influence of impact loads, it is important to know the fracture toughness in all zones of the welded joint. The crack formed in base metal or HAZ, due to dynamic or impact loads, can easily continue to propagate to the fusion line, after which its accelerated growth may occur. The fracture mechanics testing was applied to SEN (B) test specimens, which investigated cracks initiation and certain fracture mechanics parameters. Due to the significant interest in quantifying the resistance of material to initiation and propagation of cracks, the impact energy was measured with instrumented pendulum in the zone of base metal, weld metal and HAZ, at temperatures of -40 °C, -20 °C, 0 °C and 20 °C , while the fracture mechanics parameters in these zones were tested at room temperature. The impact energy tests showed high energy for initiation as well as crack propagation in weld metal and HAZ zones, while the lowest energy was in the base metal. The fracture toughness in the base metal is 86.1 MPa*$m^{1/2}$, while in HAZ and weld metal zones is 286 MPa*$m^{1/2}$ and 355 MPa*$m^{1/2}$, respectively.

Peer-review under responsibility of the ECF22 organizers.

Keywords: GMAW welding, Armor steels, Austenitic stainless steel, Fracture mechanics, Instrumented Charpy tests,

Nomenclature

J_{IC}	Critical *J*-integral,
K_{IC}	Critical fracture toughness,
R	Load ratio,
F	Force value,
a	Crack length,
δ	Opening displacement

Peer-review under responsibility of the ECF22 organizers.

1. Introduction

Armor steel belongs to the ultra-high tensile strength and hardness group of steels. Atabaki et al. (2014) described that the welding of armor steel is complicated due to the high percentage of carbon content in the base metal and the presence of defects in the form of cracks and pores in the weld metal zone, whereby fracture may be initiated in the weld metal. According to Kuzmikova et al. (2014) austenitic filler material is traditionally used for armor steel welding because of hydrogen dilution improved in an austenitic phase. It was reported by Ranjbarnodeh et. al. (2012) that after the welding process, solidification cracking may result from high thermal expansion of the austenitic stainless steel and invisible defects may be created in the weld metal zone.

For heavy structural engineering, such as armored military vehicles frequently being under the effects of impact and variable loads, mechanical properties of welded joints and the weld metal zone must be known. Due to variable loads, cracks created in the weld metal may easily propagate towards the sensitive fusion line (FL), followed by their possible rapid growth. The impact load is critical for armored vehicles, so the determination of the impact energy required for crack initiation and growth made by instrumented pendulum with Charpy V specimens, is very significant, Enrico (2016).

For armored vehicle structures safe and rational dimensioning, it is necessary to know dynamic effects extreme values and time periods. Therefore, there is a significant interest in material resistance related to crack initiation and propagation, as well as in dynamic force conditions. For the armored military vehicles reliable operation, it is very important to be able to carry out a good risk assessment of existing crack type defects. This can be achieved by fracture mechanic concepts application.

Although austenitic filler material is used the most frequently for welding and has several unusual features including its high manganese content, few articles consider the problem of its mechanical properties.

The main goal of this study was to investigate the impact energy by instrumented pendulum and fracture mechanic in welded joint. Fracture surfaces for the impact energy and fracture mechanic tests were also investigated by Scanning Electron Microscope (SEM). Subsequently, samples in the weld metal region were studied by tensile strength test, hardness measurements, metallography and chemical analysis.

2. Materials and experimental procedure

2.1 Material and welding properties

Gas metal arc welding (GMAW) and AWS ER307 solid wire is used for welding armor steel Protac 500. Welding direction is parallel to the rolling direction. Cold rolled plates 12 mm thick are cut to the required dimensions (250 x 100 mm), while V joint under the angle of 55° is prepared by Water Jet Device. Robot Kuka and Citronix 400A device was used during the welding process testing. Details on welding are shown in the article, Cabrilo et al. (2016). Robotic welding is used for human factor effect elimination, in order to allow a fine adjustment of parameters and results repeatability.

Base metal and filler material chemical composition obtained by spectro - chemical analysis are shown in Table 1. Spectro-chemical analysis was performed after the welding process.

Table 1. Chemical composition of the base metal.

Material	*Chemical composition [wt. %]*											
	C	Si	Mn	S	Cr	P	Al	Cu	Ni	Mo	V	Sn
Protac 500	0.27	1.07	0.71	0.001	0.64	0.009	0.054	0.28	1.09	0.296	0.039	0.011
AWS ER307	0.08	0.89	6.29	0.001	17.76	0.014	0.01	0.08	8.24	0.13	0.03	0.011

An amount of delta ferrite in austenitic base is determined by Feritscope. Magnetic ferrite mass fraction was measured in three zones of the welded joint: in weld metal root - lower weld metal part, then in filler zone - middle weld metal part as well as in cover passes - upper weld metal part.

2.2 Mechanical property tests

Welded joint tensile strength testing was performed in transverse direction of the weld bead. It should be noted that specimens was cut with Water Jet Device, to eliminate possibilities of thermal effects to high hardness steel. Tensile strength testing was made on servo - hydraulic testing machine Instron 8033. The loading rate was set as 0.125 mm/s until fracture took place.

2.3 Metallography and hardness testing

The microstructural examination was performed using a "Leitz-Orthoplan" metallographic microscope and a scanning electron microscope JEOL JSM 6460LV at 25 kV. The samples were ground using SiC papers, polished with a diamond paste and finally etched with a mixture HCl and HNO_3 in weld metal region, and 3% HNO_3 reagent to reveal the structure of base metal. Microhardness distribution from top to bottom along the centreline of the weld was measured for the purpose of welded metal characterization. Digital Micro Vickers Hardness Tester HVS 1000, Laiznou Huayin Testing Instrument Co, under the load of 500 g, was used in order to measure microhardeness.

2.4 Instrumented Charpy tests

Charpy impact tests in base metal, heat affected zone and weld metal, were performed on specimen's size 10 x 10 x 55 mm, with V notch of 2 mm. The test was conducted at: 20 °C, 0 °C, -20 °C and -40 °C. Load-displacement curves were obtained from the instrumented Charpy impact system attached in to the impact tester. After the test, fracture surface were examined by a SEM to observe fracture modes.

2.5 Fracture mechanic test

Three point bending specimen, SEN (B) was used for testing. Specimen's dimension 20x10x120 mm were cut by Water Jet Device, to eliminate any possibility of armor steel thermal treatment. After getting final measures in the grinding process, 5 mm long machined notch was created on specimens in the direction parallel to welding, trough weld metal zone, HAZ and base metal zone. The fatigue pre-crack was inserted before the fracture mechanic tests, which is in accordance with ASTM E399-17 (2017). The length of the fatigue pre–crack was 4.7 mm. The fatigue pre-crack was realized with a high-frequency CRACTRONIC pulsator, at a load ratio R = 0.33, followed by a constant loading frequency of 170 Hz. Experiment of fracture mechanics in the HAZ and weld metal zone was made using a single test specimen, which is in accordance with ASTM E1820-16 (2016) standard, while the crack length was determined at certain intervals. A technique of potential drop and compliance of test specimen was used to track the crack.

3. Results

3.1 Tensile testing results

While tensile characteristics were being tested, a fracture appeared in the weld metal. The tensile strength was 833 MPa, while the yield strength of 552 MPa was within the expected limits. The difference between tensile and yield strength was 311 MPa, indicating a high ductility of the weld metal.

3.2 Hardness and microstructure results

The weld metal micrograph Fig. 1 a) consist of austenite with delta ferrite. Delta ferrite becomes finer at lower heat input and cooling rate. The content of delta ferrite measured by Feritscope: in the weld root 11.7%, in the center 5.4%, in the upper part 3.2%. The base metal micrograph Fig. 1 b) in quenched and tempered condition consists of tempered and quenched martensite within the range of hardness 480-540 HB which is within accepted criteria of standard MIL-STAN-1185 (2008).

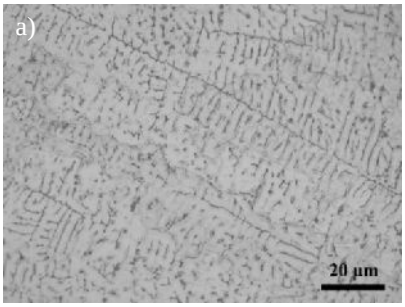

Fig. 1. a) Optical micrograph of AWS ER 307 filler.

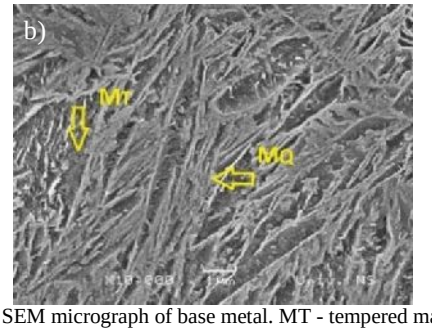

Fig. 1. b) SEM micrograph of base metal. MT - tempered martensite, MQ - quenched martensite.

Hardness rises from the center of the weld metal (WM) (190 HV), to the line of fusion and along the line on WM side has a value of 339 HV. The hardness is growing in the HAZ zone and reaches a maximum value of 521 HV, at a distance of 8 mm from the weld metal axis. After a maximum, the hardness trend is in decline with the achieved minimum hardness of 378 HV, at a distance of 10 mm from the weld metal axis. The hardness then grows and ends at a distance of 14 mm from the weld metal axis with a value of about 509 HV. The distance of 14 mm is also the limit of HAZ and base metal. The BM hardness value is 509 HV. The hardness was measured also longitudinally along the width zone of 0.5 mm following fusion line. Results from Fig. 2 b) show that fusion line hardness does not exceed 442 HV, which is very good for this zone. Hardness falls from the bottom to the upper zone, which can be the result of the heat effect that is higher in zones closest to the last passage than it is in the root passage, which is certainly affected by the already cooled additional and base metal.

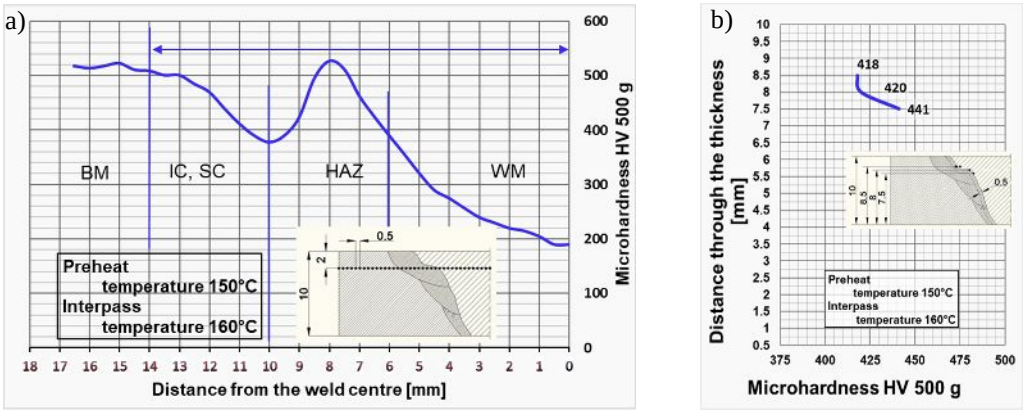

Fig. 2. a) Hardness profile for welded high hardness plate. Note: hardness was measured 2 mm under the upper surface. BM-base metal, IC-inter ritical zone, SC-sub critical zone, HAZ-heat affected zone, WM-weld metal. b) close to the fusion line.

3.3 Instrumented Charpy impact energies results

By determining the impact energy for the base metal tested at 20 °C, a diagram was obtained, Fig. 3a), with a mixed brittle and ductile fracture surface, Fig. 4 a). In order to create a crack in this zone, the measured impact energy is 28.6 J, and 5.6 J is used for propagation. The impact energy diagram for the temperature of -40 °C, Fig. 3 d) shows more pronounced brittle fracture, Fig. 4 d). At this temperature, the largest difference between the energy for creation in relation to the energy for crack propagation is of the highest percentage. The energy to create a crack of 27.8 J slightly decreased compared to the previous temperature tests, while the crack propagation energy was significantly lower and amounted only to 1.0 J.

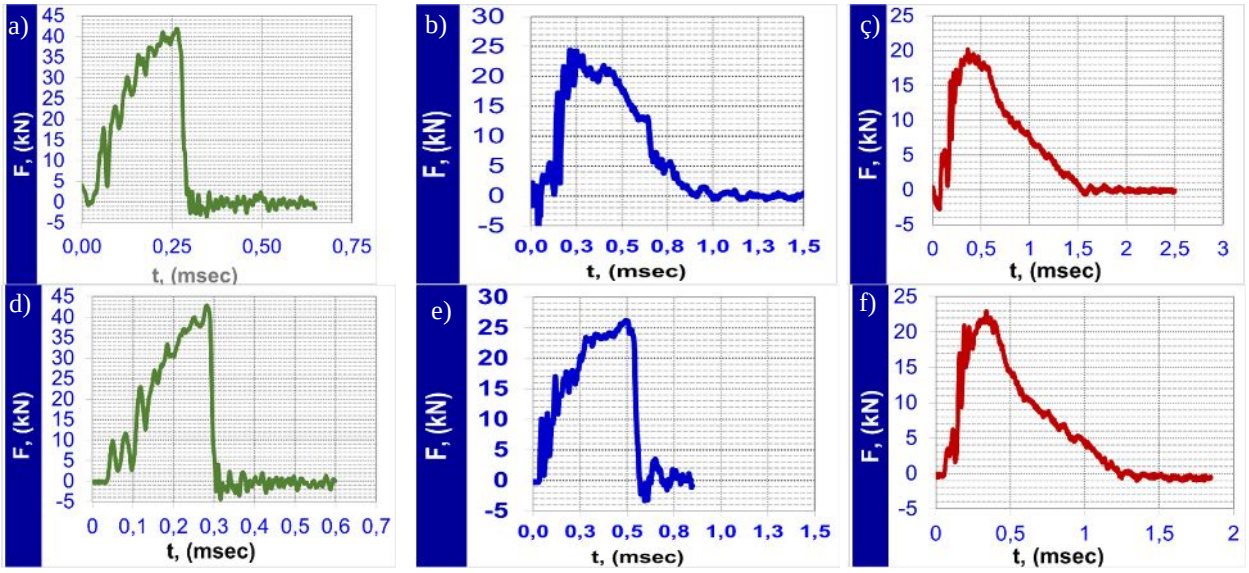

Fig. 3. The load-time (*F-t*) curve recorded by oscilloscope of Charpy impact specimens fractured at 20 °C a) base metal, b) HAZ and c) weld metal. The load-time (*F-t*) curve recorded by oscilloscope of Charpy impact specimens fractured at -40 °C d) base metal, e) HAZ and f) weld metal.

Determining the fracture energy for fusion line tested at 20°C, the diagram was obtained, Fig. 3 b), with the prevailing ductile fracture surface, Fig. 4 b). For creation of crack in this zone, the measured impact energy is 45.7 J, and 29.6 J is used for growth. Diagram of the impact energy for temperature of -40°C, Fig. 3 e) is a purely brittle fracture, Fig. 4 e). The crack creation energy of 27.7 J slightly decreased compared to tests at previous temperatures, while the crack propagation energy was significantly lower and amounted to 12.3 J.

By determining the impact energy for the weld metal examined at 20 °C, a diagram with a typical ductile fracture surface was obtained, Fig. 3 c) and 4 c). In order to create a crack in this zone, the measured impact energy was 29.0 J, while significantly more energy was used for crack propagation, in the amount of 55.4 J. The diagram of energy impact for the temperature of -40 °C, Fig. 3 f) and 4 f) is a ductile fracture. The energy to create a crack of 24.2 J significantly decreased compared to tests at previous temperatures, while the crack propagation energy was slightly lower and amounted to 37.3 J.

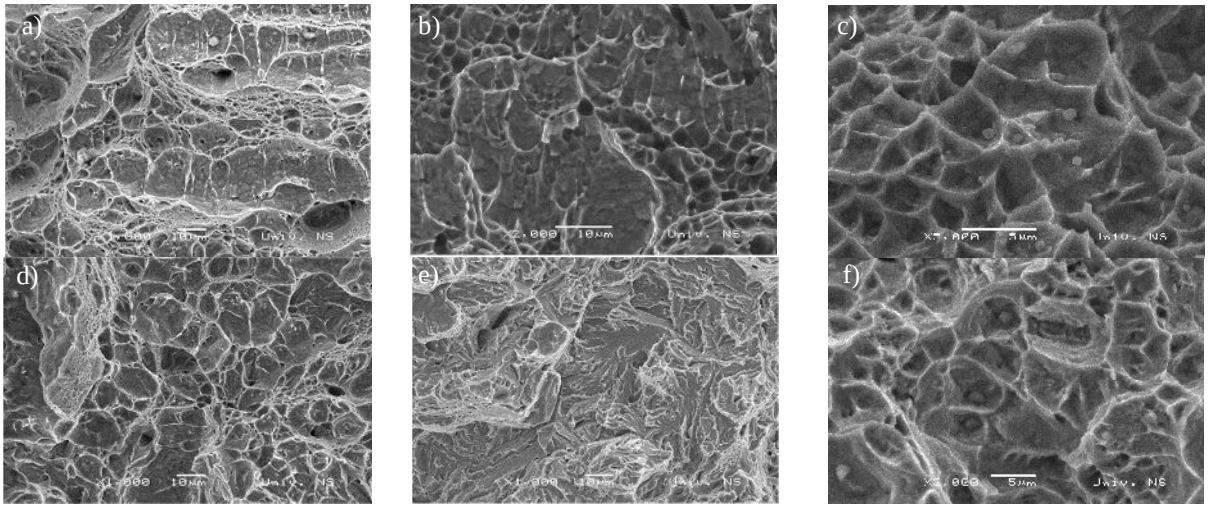

Fig 4. SEM fractograph of Charpy impact specimens fractured at 20 °C a) base metal, b) HAZ and c) weld metal. SEM fractograph of Charpy impact specimens fractured at -40 °C d) base metal, e) HAZ and f) weld metal.

3.4 Fracture mechanic results

The mean value of fracturing mechanics results is shown in Table 2.

Table 2. Results of testing the critical *J-integral*, J_{IC}, and the critical stress intensity factor, K_{IC}.

Specimen	*Critical J-integral* J_{IC}	*Critical fracture toughness* K_{IC}
	[kJ/m^2]	[MPa*m$^{1/2}$]
Specimen BM		86.1
Specimen HAZ	355	286
Specimen WM	545	355

For the crack in base metal, the thickness requirement is met, i.e. the mean value of tension concentration factor, K_{IC}, is 86.1 MPa*m$^{1/2}$.

Results of testing by the potential drop and compliance technique in the zone of HAZ and weld metal with one test specimens are shown in Fig. 5 a) and 6 a). The critical value of *J - integral*, J_{IC}, is obtained by the intersection of the regression line and the blunting line, and is 355 kJ/m^2 for the HAZ and the weld metal respectively. Based on the critical J_{IC} integral, the fracture toughness, K_{IC}, is indirectly determined, amounting 286 MPa*m$^{1/2}$ and 355 MPa*m$^{1/2}$.

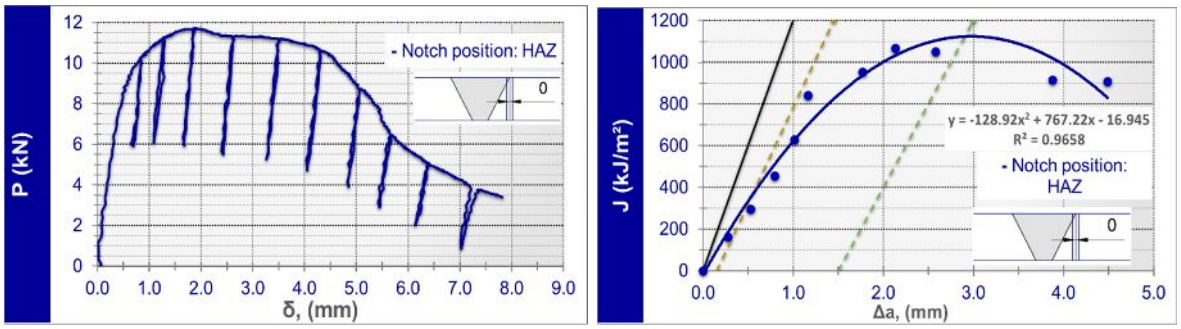

Fig. 5. Diagrams a) F – δ and b) J – Δa for the specimen with a notch in HAZ.

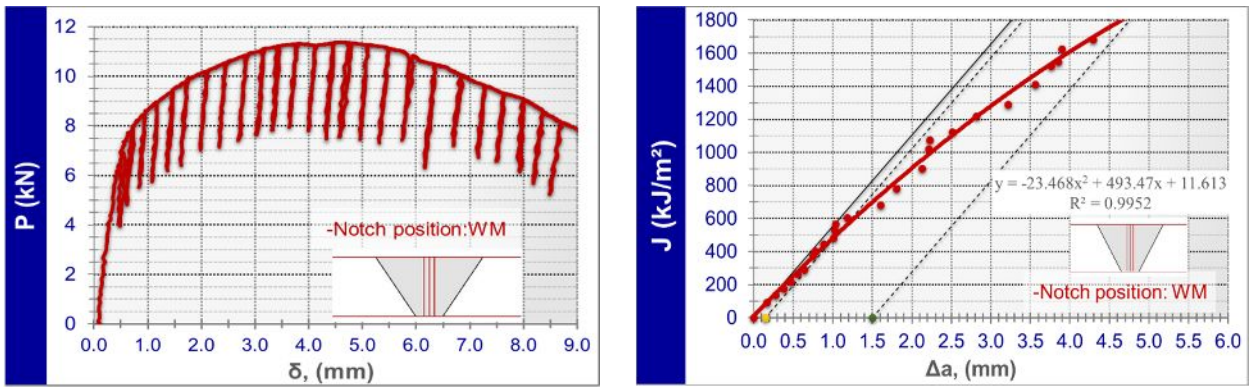

Fig. 6. *Diagrams a) F – δ and b) J – Δa for the specimen with a notch in weld metal.*

4. Discussion

It is known that welded joints are very heterogeneous, since they include weld metal, heat affected zone and base metal. Hardness is therefore defined by the zone of minimum hardness, which in the case of armor steel welding with austenitic filler material, is the weld metal zone. Armor steel welded joints are expected to have a tensile strength not lower than 550 MPa, in order to satisfy the requirements of MIL-STD-1185. The tensile strength achieved in this research of 833 MPa is rather high for austenitic filler material and significantly higher than the tensile strength obtained by Magudeeswaran et al. (2014).

Quality indicators of the welded joint are results of impact energy test with the position of the notch on the fusion line. Based on this value, the final grade of welded joint quality of armored steel can be given. The impact energy value at all temperatures indicates that the crack propagation was very difficult. However, it can be concluded that there has been a pronounced drop in the impact energy with a drop in the test temperature. With a decrease in temperature from 20 °C to -40 °C, the energy impact drop is from 75.3 J to 40.0 J. At a temperature of 20 °C, the ratio of energy for initiation and propagation is 70:30. On the energy - time curve, after the initiation energy, a mild drop occurred, which indicates that more energy was needed for crack propagation. The impact energy data can be linked to the obtained hardness values measured around the fusion line, as the impact energy increases with the decrease in the hardness value. As Fig. 2 b) shows, the hardness around the fusion line range from 418 HV to 441 HV, indicating that bainite increases the energy for crack initiation and propagation. Fracture area fractography at -20 °C and -40 °C shows the prevailing brittle fracture.

Reducing the impact energy in the weld metal from 84.4 J to 64.4 J, obtained at temperatures of 20 °C and -40 °C, is noticeable. A large drop is characteristic of ductile materials, which is in agreement with Hu et al. (2018), because at lower temperatures, the energy needed to crack propagation is reduced. The SEM tests showed ductile fracture at all test temperatures. On the load - time curve, after the energy for initiation, a very slight drop, characteristic of ductile fracture, occurred. When it comes to temperatures of -40 °C, the ratio of energy for propagation and crack initiation remained the same, 34:66% in favor of propagation energy. After achieving the initiation energy of 20.8 J, there is a slight fall in the curve and the required energy for propagation is 40.7 J. The impact energies at temperatures of -40 °C and 20 °C are achieved due to an optimum hardness of 200 HV and high content of nickel and manganese. The impact energy of 56 J required for crack initiation is typical of ductile materials. At a temperature of -40 °C, the initiation energy decreased considerably, but still remained high. SEM microscopy indicates that the fracture was ductile at all investigated temperatures. In relation to the metallography shown in the study Magudeeswaran et al. (2014) segregated δ - ferrite is noticeable, while in the results of this work it is evenly distributed, which can be the cause of higher impact energy regarding both tests. Thicker and more uniform arrangement of δ -ferrite was obtained by the REL method compared to the MIG procedure in the Magudeeswaran et al. (2010) study. The amount of δ - ferrite measured in this test is approximately the same with REL welding in the study with the notion that the arrangement of δ - ferrite in this test is even more uniform.

HAZ showed a good and balanced relationship between toughness and hardness of the fracture. The calculated fracture toughness value, K_{IC} = 285 MPa $m^{1/2}$. Comparing the fracture toughness value of this crack position with the crack in the base metal, an evident difference of 200 MPa $m^{1/2}$ can be established. K_{IC} fracture toughness, due to the linear-plastic behavior, was obtained indirectly on the basis of the *J-R* curve. The *J-R* curve was obtained by a potential dropping technique, using a single test specimen. While the critical value of the J_{IC} for cracking initiation, 0.15 mm in length, is $J_{0.15}$ mm = 355 kJ/m^2, the fracture surface is mixed ductile brittle with a visible extension zone.

There is very little data in the literature on the fracture toughness for the class 500 HB armored steel, which includes Protac 500. The fracture toughness value of 86 MPa*$m^{1/2}$, obtained in this test, enables the determination of a critical load for the size of crack that can appear in the base metal. Requirements of the standards were met on all five tested specimens, with no pop-ins in the specimens, while the crack propagated steadily, which means that there are no brittle areas through which the crack progresses faster. However, it is somewhat lower in comparison to the same class of armored steel, Bisalloy 500, where it was obtained for K_{IC} in the longitudinal direction 121 MPa*$m^{1/2}$, and in the cross-section 111 MPa*$m^{1/2}$ in the work of Shah Khan (1998). The fractogram examined by SEM indicates that in this case there is a uniform stretching zone along the entire sample. The base metal showed a good and balanced relationship between the toughness and hardness of the fracture. The lowest fracture toughness in this zone, relative to all other zones of the welded joint is expected, given the martensite structure of the base metal.

In the weld metal, value of the critical *J integral*, J_{IC}, is 545 kJ/m2. In comparison with other notch positions, the crack propagation resistance in this zone is the highest. A good combination of fracture toughness and hardness was achieved with a fine skeleton of δ - ferrite in the austenite matrix, Fig. 1a). The amount of δ - ferrite is 6.8%. The cooling rate during the welding process, and the chemical composition of additional material have certain effect on the quantity, morphology and homogeneity of δ -ferrite in the austenite matrix. The high J_{IC} value is achieved by the optimum hardness, as well as the high content of nickel and manganese. More pronounced resistance to crack propagation in this area can be caused by the influence of nickel. Nickel stabilizes austenite and plays an important role in the control of microstructure. Pilhagen et al. (2014) described that with the increase in nickel, toughness of the weld metal fracture increases.

Fracture toughness of fatigue crack position in the base metal shows clear brittle fracture characteristics. Based on the results, it was shown that fracture toughness is higher in the coarse area of the HAZ than in the base metal area. It can be noted that the fracture toughness, K_{IC}, increases with the approach of weld metal zone. The fracture toughness, K_{IC}, in the HAZ increased drastically in relation to the base metal. The fracture toughness value, K_{IC}, is closer to the weld metal value than the value of the base metal.

5. Conclusions

On the basis of the results presented in this work, the following conclusions may be made:

1. Tensile strength of weld metal in the specimen welded with austenitic filler metal reached 833 MPa, which is greater than results published for the same filler metal in researches of manual welding.

2. Austenitic filler material shows a significant decrease in impact energy, followed by reduction in testing temperature. The results at room temperature showed high energies for crack initiation 56 J and propagation 29 J. The results at -40 °C indicate that significantly less energy is required for crack initiation 41 J, while a small drop was observed for propagation 21 J. During SEM analysis of the fracture surface, small high density dimples were clearly visible. Morphology of the fracture surface at -40 °C indicates a mixed brittle ductile fracture. The results at room temperature showed high energy absorptions for crack initiation (48 J) and propagation (27 J). The results at -40 °C indicated that significantly less energy is required for crack initiation (29 J) and propagation (11 J). The lowest energy for initiation (30 J) and crack propagation (5 J) at room temperature has a base metal. In this zone, a slight decrease in the energy of the impact between the test temperature of 20 ° C and -40 ° C.

3. Fracture toughness value of 86 MPa*$m^{1/2}$ is slightly lower than in the Class 500 of armored steel. Results of calculation show that HAZ has triple fracture toughness in comparison to the base metal. The highest fracture toughness is in the weld metal, four times higher than in the base metal.

Acknowledgements

The authors would like to thank PhD Zijah Burzic, and Military Technical Institute for Mechanical Testing

This study was financially supported by the Ministry of Education, Science and Technological Development of the Republic of Serbia through the Project Nos. ON 174004.

References

Atabaki, M., M., Ma, J., Yang, G., Kovacevic, R., 2014. Hybrid laser/arc welding of advanced high strength steel in different butt joint configurations, in Material and Design, pp. 573–587.

ASTM E399-17, 2017. Standard Test Method for Linear-Elastic Plane-Strain Fracture Toughness KIc of Metallic Materials, ASTM International, West Conshohocken, PA, 2017.

ASTM E1820-16, 2016. Standard Test Method for Measurement of Fracture Toughness, ASTM International, West Conshohocken, PA, 2016.

Bernetic, J., 2013. Development of model for predicting hardenability of high strength low alloy steels, Ph. D. Thesis. Ljubljana, January.

Cabrilo, A., Geric, K., 2016. Weldability of High hardness armour steel, in Advance Material Research, pp. 79-84.

Enrico, L., 2016. Estimating dynamic ultimate tensile strength from instrumented Charpy data, in Material and Design, pp. 437–443.

Hu, J., Du, L. X., Xu, W., Zhai, J. H., Dong, Y., Liu, Y.,J., Misra, R., D., K., 2018. Ensuring combination of strength, ductility and toughness in mediummanganese steel through optimization of nano-scale metastable austenite, Materials Characterization, pp. 20–28.

Kuzmikova, L., Norrish, J., Li, H., Callaghan, M., 2011. Research to establish a systematic approach to safe welding procedure development using austenitic filler material for fabrication of high strength steel, 16th International Conference on the Joining of Materials paper 1-13.

Magudeeswaran, G. Balasubramanian, V., R., 2014. Effect of welding processes and consumables on fatigue crack growth behaviour of armour grade quenched and tempered steel joints, Defence Technology, pp. 47-59.

Magudeeswaran, G., Balasubramanian, V., Sathyanarayanan, S., Madhusudhan, G., R., 2010. Dynamic Fracture Toughness of Armour Grade Quenched and Tempered Steel Joints Fabricated Using Low Hydrogen Ferritic Fillers, Journal of Iron and Steel Research, International, pp. 51-56.

MIL-STD-1185. 2008. Department of defense manufacturing process standard: welding, high hardness armor; [SUPERSEDES MIL-W-62162].

Pilhagen, J., Sandström, R., 2014. Influence of nickel on the toughness of lean duplex stainless steel welds. Materials Science & Engineering, A, pp. 49–57.

Ranjbarnodeh, E., Pouraliakbar, H., Kokabi, A. H., 2012. Finite Element Simulation of Carbide Precipitation in Austenitic Stainless Steel 304. International Journal of Mechanical Application, pp. 117–123.

Shah Khan, M., Z., Alkemade, S., J. and Weston, G., M., 1998. Fracture Studies and High Hardness Bisalloy 500 Steel. Martime Platform Division Aeronautical and Martime Research Labaratory DSTO-RR-0130.